Research Article Open Access

Asim Aziz*, Wasim Jamshed, and Taha Aziz

Mathematical model for thermal and entropy analysis of thermal solar collectors by using Maxwell nanofluids with slip conditions, thermal radiation and variable thermal conductivity

https://doi.org/10.1515/phys-2018-0020
Received July 30, 2017; accepted November 26, 2017

Abstract: In the present research a simplified mathematical model for the solar thermal collectors is considered in the form of non-uniform unsteady stretching surface. The non-Newtonian Maxwell nanofluid model is utilized for the working fluid along with slip and convective boundary conditions and comprehensive analysis of entropy generation in the system is also observed. The effect of thermal radiation and variable thermal conductivity are also included in the present model. The mathematical formulation is carried out through a boundary layer approach and the numerical computations are carried out for Cu-water and TiO_2-water nanofluids. Results are presented for the velocity, temperature and entropy generation profiles, skin friction coefficient and Nusselt number. The discussion is concluded on the effect of various governing parameters on the motion, temperature variation, entropy generation, velocity gradient and the rate of heat transfer at the boundary.

Keywords: Solar energy; thermal collectors; entropy generation; Maxwell-nanofluid; thermal radiation; partial slip; variable thermal conductivity

PACS: 44.20.+b, 44.40.+a, 47.10.A-

***Corresponding Author: Asim Aziz:** College of Electrical and Mechanical Engineering, National University of Sciences and Technology, Rawalpindi, 46070, Pakistan, E-mail: aaziz@ceme.nust.edu.pk, Tel: +92-51-9247541
Wasim Jamshed: Department of Mathematics, Capital University of Science and Technology, Islamabad, 44000, Pakistan
Taha Aziz: School of Computer, Statistical and Mathematical Sciences, North-West University, Potchefstroom Campus, Private Bag X6001, Potchefstroom 2531, South Africa

1 Introduction

Solar energy is the cleanest, renewable and most abundant source of energy available on earth. The amount of electricity that can be produced by solar energy is 4×10^{15} megawatt which is 200 times more then the global consumption of the electricity [1]. The main use of solar energy is to heat and cool buildings, heat water and to generate electricity [2–5]. There are two types of solar energy collection systems, the photovoltaic systems and the solar thermal collectors. The solar thermal collectors consists of three main parts, the solar energy collection system, the heat storage medium and the heat circulation system. Most popular types of solar thermal collectors are parabolic dish collectors, parabolic trough and power tower systems [1]. The recent research in the field of solar energy has been focused to increase the efficiency of solar thermal collector systems. The efficiency of any solar thermal system depend on two key parameters, the thermophysical properties of the operating fluid and the geometry/length of the system in which fluid is flowing. The properties of the operating fluids include viscosity, density, thermal conductivity and specific heat at high temperature as well as the velocity of the flow [6, 7].

The use of nanofluids instead of ordinary fluids is the key area of research to improve the performance of solar thermal collectors. However it is important to select the type of the nanoparticles, nanoparticles volumetric concentration in the base fluid and the nanofluid thermophysical properties. Chaji *et al.* [8] experimented on flat thermal solar collectors using TiO_2-water nanofluid with the aim to study the collectors efficiency corresponding to nanoparticles concentration and the flow rate. They found that by adding the nanoparticles to water, the collector efficiency increases between 2.6% and 7% relative to the base fluid. Ghasemi and Ahangar [9] numerically investigated the thermal field and thermal efficiency of parabolic trough collectors with Cu-water nanofluid and conclude that the solar collectors with nanofluid is more efficient when compared with conventional collectors. The inclusion of copper nanoparticles considerably increase the heat gain capacity of solar collector. Sharma and Kundan [10] in their experimental setup for parabolic solar collector compare the efficiency of ordinary fluid with aluminium-water nanofluid with copper oxide nanofluid. It is concluded that the aluminium water nanofluid improve the efficiency of solar collector between $1 - 2.55\%$ whereas the use copper oxide nanofluid the efficiency is improved by $0.95 - 3.05\%$. Bellos *et al.* [11] presented that the efficiency of parabolic trough collectors with sine geometry improved by 4.25% if nanofluids are used as operating fluids instead of thermal oil or pressurized water. Recently [12, 13] independently used carbon nanotube nanofluids as working fluids to examine the efficiency of U-tube thermal solar collectors. The use of carbon nanotube nanofluids not only improve the efficiency of solar collectors they also reduce the CO_2 emissions. Kim *et al.* [13] also compared the efficiency of carbon nanotube nanofluids with Al_2O_3, CuO, SiO_2 and TiO_2 nanofluids. Their results indicated that the greatest efficiency was obtained at 62.8% when when carbon nanotube nanofluids are used. Finally the review article of Muhammad *et. al* [14] covered almost all the literature of past ten years on use of nanofluids and enhancement in thermal efficiency of solar collectors.

In all aforementioned studies authors considered Newtonian fluid model for convective transport of nanofluids. However, in real situation nanofluids do not have the characteristics of Newtonian fluids hence it is more reasonable to consider them as non-Newtonian fluids. Ellahi *et al.* [15] used OHAM and investigated the exact solution of mixed convection Power-law nanofluid of the copper nanoparticles and using the Brinkman nanofluid model. They found that the velocity profile of shear thinning fluids falls when nanoparticle volume fraction is increases. Ellahi *et al.* [16] considered the Brinkman nanofluid model to investigate the impact of $HFE - 7100$ fluid over a wedge the influence of porous medium, entropy generation and three different type of shape nanoparticles such as needle-shaped, disk-shaped, sphere-shaped are taken into consideration. They concluded that needle-shaped nanoparticles results is the greatest temperature in the boundary layer while the lowest temperature are observed in the case of sphere-shaped nanoparticles. It is also obtained when one chose disk-shaped particles and $HFE - 7500$ fluid shows the greater heat transfer ability as compared with rest of the nanoparticles and the highest entropy is found by the needle-shaped nanoparticles as compared to other nanoparticle shapes. Sheikholeslami *et al.* [17] employed Koo-Kleinstreuer-Li correlation for MHD nanofluid flowing over two vertical permeable sheets for Al_2O_3-water under the influence of free convection is investigated. They used the Runge-Kutta method for the numerical solutions and discussed the effects of various physical parameters on nanofluids. The results indicated that the enhancement in heat transfer is an increasing function of Hartman number. Esfahani *et al.* [18] investigated an entropy generation for the Copper-water nanofluid flow through a wavy channel over heat exchanger plat , The results indicated that the enhancement in viscous entropy generation with greater Reynolds number becomes more prominent as non-dimension amplitude rises. In addition to the above, the non-Newtonian nanofluid models are well discussed in [19–21].

Examination of solar collectors in terms of their exergy and its efficiency and entropy generation has been carried out in [22–24]. The effects of heat transfer irreversibilities on the account of exergy obtained from the solar collectors systems was investigated by Bejan [25]. A comparison between the flat plate and evacuated tube collectors as a function of exergy was carried out by Suzuki[26]. Farzad *et al.*[27] scrutinized both exergy analysis and energy of a flat plate solar collector. Luminosu and Fara [28] suggested exergy analysis of a flat plate solar collector based on the assumption that fluid inlet temperature is equal to ambient temperature. The analysis optimum values of mass flow rate, absorber plate area, and maximum exergy efficiency of a flat plate collector was carried out by Farahat *et al.*[29]. Nasrin *et al.*[30] considered radiative heat flux effects on the direct absorption of the solar collector and studied the heat transfer and collector efficiency. The use of graphene based nanofluid in the flat plate solar collector exergy efficiency analysis was carried out by Said *et al.*[31]. Further detail regarding the entropy generation analysis in solar collectors can be found in [32–34]. In all aforementioned studies authors considered Newtonian fluid model for convective transport of nanofluids. However, in real situation nanofluids do not have the characteristics of Newtonian fluids hence it is more reasonable to consider them as non-Newtonian fluids. The flow and heat transfer analysis of non-Newtonian models of nanofluids in solar collectors will provide researchers the better understanding of thermal characteristics of nanofluids and efficiency measurement. Some authors do considered non-Newtonian models for the nanofluids under different thermophysical situations, for example, [35–41]. To the best of author's knowledge no research is conducted to study the combined effect of MHD non-Newtonian Maxwell nanofluid with slip and convective boundary conditions, thermal radiation and temperature dependent thermal conductivity on velocity, temperature distribution and entropy generation of the system. The flow is induced by a non-uniform stretching of the porous sheet and the uniform magnetic field is applied in the transverse direction to the flow. The numerical computations are carried for Cu-water and TiO_2-water nanofluids and results are concluded on the effect of various governing parameters on the motion, temperature and entropy generation of Maxwell nanofluid.

2 Mathematical formulation

We consider an unsteady, two-dimensional laminar flow with heat transfer of an incompressible electrically conducting non-Newtonian Maxwell nanofluid over a porous stretching sheet. The flow is generated due to the stretching of sheet with non-uniform velocity

$$U_w(x,t) = \frac{cx}{1-\varpi t}, \tag{2.1}$$

where c is the initial stretching rate and $\frac{1}{1-\varpi t}$ (with $\varpi t < 1$) is the effective stretching rate. The surface of the plate is insulated and partial slip and convective conditions has been invoked at the boundary. For convenience, the leading edge of the plate is assumed at $x = 0$ and is considered along the x-axis. A uniform magnetic field of strength $B(t) = \frac{B_0}{\sqrt{1-\varpi t}}$ is applied in the transverse direction to the flow and the induced magnetic field is considered negligible as compared to applied magnetic field. The temperature of the plate is $T_w(x,t) = T_\infty + \frac{cx}{1-\varpi t}$ and T_∞ is the temperature outside the boundary layer. Thermal conductivity of the nanofluid is to vary as a linear function of temperature, T. This assumption is valid because thermal properties of nanofluids change significantly with rise in temperature, type of nanoparticles, pressure etc. Finally, the non-Newtonian Maxwell nanofluid is considered optically thick and radiation only travel a short distance. Therefore radiative heat transfer is taken into account and Rosseland approximation is utilized for the radiation effects. The schematic diagram of the mathematical model under consideration is presented in Figure (1).

The governing equations under boundary layer approximation for the flow of Maxwell nanofluid along with heat transfer are obtained as (see for example, Mukhopadhyay [42])

$$\frac{\partial u}{\partial x} + \frac{\partial v}{\partial y} = 0, \tag{2.2}$$

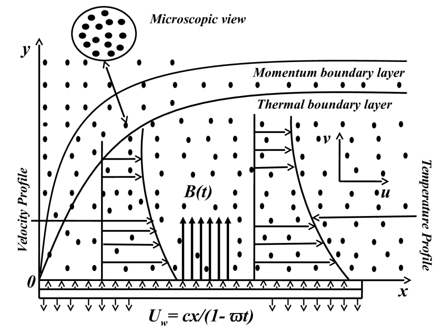

Figure 1: Schematic diagram of solar collector

$$\begin{aligned}\frac{\partial u}{\partial t} + u\frac{\partial u}{\partial x} + v\frac{\partial u}{\partial y} &= \frac{\mu_{nf}}{\rho_{nf}}\frac{\partial^2 u}{\partial y^2} \\ &- \lambda\left[u^2\frac{\partial^2 u}{\partial x^2} + v^2\frac{\partial^2 u}{\partial y^2} + 2uv\frac{\partial^2 u}{\partial x\partial y}\right] \\ &- \frac{\sigma_{nf}B^2(t)u}{\rho_{nf}} - \frac{\mu_{nf}}{\rho_{nf}k}u,\end{aligned} \tag{2.3}$$

$$\begin{aligned}\frac{\partial T}{\partial t} + u\frac{\partial T}{\partial x} + v\frac{\partial T}{\partial y} &= \frac{1}{(\rho C_p)_{nf}}\left[\frac{\partial}{\partial y}(\kappa^\star_{nf}(T)\frac{\partial T}{\partial y})\right] \\ &- \frac{1}{(\rho C_p)_{nf}}\left[\frac{\partial q_r}{\partial y}\right].\end{aligned} \tag{2.4}$$

The boundary conditions for the present model are

$$\begin{aligned}&u(x,0) = U_w + W_1\mu_{nf}\left(\frac{\partial u}{\partial y}\right), \quad v(x,0) = V_w, \\ &-k_f\left(\frac{\partial T}{\partial y}\right) = h_f(T_w - T),\end{aligned} \tag{2.5}$$

$$u \to 0, \quad T \to T_\infty \text{ as } y \to \infty. \tag{2.6}$$

Here, u and v are velocities in x and y directions respectively, t is the time, μ_{nf} is the dynamic viscosity of the nanofluid, ρ_{nf} is the nanofluid density, σ_{nf} is the electrical conductivity of nanofluid. $\lambda = \lambda_0(1-\alpha t)$ is the thermal relaxation time of the period, λ_0 is a constant. q_r is the radiative heat flux, $(C_p)_{nf}$ and $\kappa^\star_{nf}$ are the specific heat capacity and the thermal conductivity of nanofluid respectively. V_w represents the porosity of the stretching surface, $W_1 = W_0\sqrt{1-\varpi t}$ is the velocity slip factor with W_0 is an initial slip parameter.

In the present study we consider (for details see for example, [43–45])

$$\begin{aligned}&\mu_{nf} = \mu_f(1-\phi)^{-2.5}, \quad \kappa^\star_{nf}(T) = k_{nf}\left[1 + \epsilon\frac{T - T_\infty}{T_w - T_\infty}\right], \\ &(\rho C_p)_{nf} = (1-\phi)(\rho C_p)_f + \phi(\rho C_p)_s,\end{aligned} \tag{2.7}$$

$$\frac{\rho_{nf}}{\rho_f} = (1-\phi) + \phi\frac{\rho_s}{\rho_f},$$
$$\frac{\sigma_{nf}}{\sigma_f} = \left[1 + \frac{3(\frac{\sigma_s}{\sigma_f}-1)\phi}{(\frac{\sigma_s}{\sigma_f}+2)-(\frac{\sigma_s}{\sigma_f}-1)\phi}\right],$$
$$\frac{\kappa_{nf}}{\kappa_f} = \left[\frac{(\kappa_s+2\kappa_f)-2\phi(\kappa_f-\kappa_s)}{(\kappa_s+2\kappa_f)+\phi(\kappa_f-\kappa_s)}\right]. \tag{2.8}$$

Here, ϕ and k_{nf} are nanoparticle volume concentration coefficient and thermal conductivity respectively. μ_f, ρ_f and $(C_p)_f$, σ_f and κ_f are dynamic viscosity, density, specific heat capacity, electrical conductivity and thermal conductivity of the base fluid. ρ_s, $(C_p)_s$, σ_s and κ_s are the density, specific heat capacity, electrical conductivity and thermal conductivity of the nanoparticles. Using Rosseland approximation (Brewster [46]), we may write

$$q_r = -\frac{4\sigma^\star}{3k^\star}\frac{\partial T^4}{\partial y}, \tag{2.9}$$

where, $\sigma^\star$ is the Stefan Boltzmann constant and $k^\star$ is the mean absorption coefficient. It is assumed that the difference in temperature within the flow is such that T^4 may be expanded as a Taylor series about free stream temperature T_∞ and considering only the linear terms, we get

$$T^4 \cong 4T_\infty^3 T - 3T_\infty^4. \tag{2.10}$$

Equation (2.9) together with equation (2.10) becomes

$$\frac{\partial q_r}{\partial y} = -\frac{16T_\infty^3\sigma^\star}{3k^\star}\frac{\partial^2 T}{\partial y^2}. \tag{2.11}$$

3 Similarity solution of the problem

To solve the governing system of partial differential equations (2.2)-(2.6), we introduce stream functions ψ, such that

$$u = \frac{\partial \psi}{\partial y}, \qquad v = -\frac{\partial \psi}{\partial x}. \tag{3.1}$$

Here $\psi(x,y)$ is the stream function and the similarity variables are defined as

$$\eta(x,y) = \sqrt{\frac{c}{\nu_f(1-\varpi t)}}y, \quad \psi(x,y) = \sqrt{\frac{\nu_f c}{(1-\varpi t)}}xf(\eta),$$
$$\theta(\eta) = \frac{T-T_\infty}{T_w-T_\infty}. \tag{3.2}$$

Upon substitution of Eqs.(3.1)-(3.2) together with Eqs. (2.7)-(2.11), the governing boundary value problem (2.2)-(2.6), reduced into a self similar system of ordinary differential equation

$$A\left(\frac{\eta}{2}f'' + f'\right) + f'^2 - ff'' - \frac{f'''}{\phi_1\phi_2} + \beta\left(f^2f''' - 2ff'f''\right)$$
$$+ \frac{\phi_4}{\phi_2}Mf' + \frac{1}{\phi_1\phi_2}Kf' = 0, \tag{3.3}$$

$$\theta''\left(1 + \epsilon\theta + \frac{1}{\phi_5}PrNr\right) + \epsilon\theta'^2$$
$$+ Pr\frac{\phi_3}{\phi_5}\left[f\theta' - f'\theta - A(\theta + \frac{\eta}{2}\theta')\right] = 0, \tag{3.4}$$

and boundary conditions

$$f(0) = S, \qquad f'(0) = 1 + \frac{\Lambda}{\phi_1}f''(0), \quad \theta'(0) = -B_i(1-\theta(0)), \tag{3.5}$$

$$f'(\eta) \to 0, \qquad \theta(\eta) \to 0, \text{ as } \eta \to \infty, \tag{3.6}$$

where

$$\phi_1 = (1-\phi)^{2.5}, \quad \phi_2 = \left(1 - \phi + \phi\frac{\rho_s}{\rho_f}\right),$$
$$\phi_3 = \left(1 - \phi + \phi\frac{(\rho C_p)_s}{(\rho C_p)_f}\right), \tag{3.7}$$

$$\phi_4 = \left(1 + \frac{3(\frac{\sigma_s}{\sigma_f}-1)\phi}{(\frac{\sigma_s}{\sigma_f}+2)-(\frac{\sigma_s}{\sigma_f}-1)\phi}\right),$$
$$\phi_5 = \left(\frac{(k_s+2k_f)-2\phi(k_f-k_s)}{(k_s+2k_f)+\phi(k_f-k_s)}\right). \tag{3.8}$$

In above equations, prime denotes the differentiation with respect to η, $A = \frac{\varpi}{c}$ is the unsteadiness parameter, $\beta = c\lambda_0$ is the Maxwell parameter, $M = \frac{\sigma_f B_o^2}{c\rho_f}$ is the magnetic parameter, $K = \frac{\nu_f(1-\varpi t)}{ck}$ is the porous medium parameter, $Pr = \frac{\nu_f}{\alpha_f}$ is the Prandtl number, $\alpha_f = \frac{\kappa_f}{(\rho C_p)_f}$ is the thermal diffusivity parameter, $Nr = \frac{16}{3}\frac{\sigma^\star T_\infty^3}{\kappa^\star \nu_f(\rho C_p)_f}$ is the thermal radiation parameter, $S = -V_w\sqrt{\frac{1-\varpi t}{\nu_f\, c}}$ is the mass transfer parameter, $\Lambda = W_0\sqrt{\frac{c}{\nu_f}}\mu_f$ is the velocity slip parameter and $B_i = \frac{h_f}{k_f}\sqrt{\frac{\nu_f(1-\varpi)t}{c}}$ is the sheet convection parameter or so-called Biot number.

The nonlinear system of ordinary differential equations (3.3)-(3.4), arising from mathematical modeling of physical system of nanofluid flow in solar collector are difficult to solve analytically. Therefore, Keller box method [47] scheme is employed to find the approximate solution of system. This method is unconditionally stable with a second order convergence.

4 Numerical solution of the problem

The flow chart of the Keller box method [47] is as follows

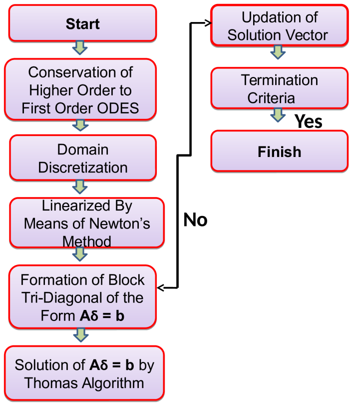

Figure 2: Flow sheet of Keller box method

The first step of the method is to convert the equations (3.3)-(3.6) into a system of five first order ordinary differential equations

$$u = f', \tag{4.1}$$

$$v = u', \tag{4.2}$$

$$t = \theta', \tag{4.3}$$

$$A\left(\frac{\eta}{2}v + u\right) + u^2 - fv - \frac{v'}{\phi_1\phi_2} + \beta\left(f^2v' - 2fuv\right) + \frac{\phi_4}{\phi_2}Mu + \frac{1}{\phi_1\phi_2}Ku = 0, \tag{4.4}$$

$$t'\left(1 + \epsilon\theta + \frac{1}{\phi_5}PrNr\right) + \epsilon t^2 + Pr\frac{\phi_3}{\phi_5}\left[ft - u\theta - A(\theta + \frac{\eta}{2}t)\right] = 0, \tag{4.5}$$

With the newly introduced variables, the boundary condition becomes:

$$f(0) = S, u(0) = 1 + \frac{\Lambda}{\phi_1}v(0), t(0) = -Bi(1 - \theta(0)),$$
$$u(\infty) \to 0, \theta(\infty) \to 0. \tag{4.6}$$

Then the derivatives are approximated by the central differences and averages centered at the midpoints of the mesh, defined by,

$$\eta_0 = 0; \quad \eta_j = \eta_{j-1} + h, \quad j = 1, 2, 3, \ldots, J-1 \quad \eta_J = \eta_\infty$$

and the derivatives are approximated by the central differences. The system of ODEs (4.1)-(4.6) is then converted to the following system of nonlinear algebraic equations.

$$\frac{u_j + u_{j-1}}{2} = \frac{f_j - f_{j-1}}{h}, \tag{4.7}$$

$$\frac{v_j + v_{j-1}}{2} = \frac{u_j - u_{j-1}}{h}, \tag{4.8}$$

$$\frac{t_j + t_{j-1}}{2} = \frac{\theta_j - \theta_{j-1}}{h}, \tag{4.9}$$

$$\begin{aligned}&A\left\{\left(\frac{u_j + u_{j-1}}{2}\right) + \frac{\eta}{2}\left(\frac{v_j + v_{j-1}}{2}\right)\right\} + \left(\frac{u_j + u_{j-1}}{2}\right)^2\\ &- \left(\frac{f_j + f_{j-1}}{2}\right)\left(\frac{v_j + v_{j-1}}{2}\right) - \frac{1}{\phi_1\phi_2}\left(\frac{v_j - v_{j-1}}{h}\right)\\ &+ \beta\left(\left(\frac{f_j + f_{j-1}}{2}\right)^2\left(\frac{v_j - v_{j-1}}{h}\right)\right.\\ &\left.-2\left(\frac{f_j + f_{j-1}}{2}\right)\left(\frac{u_j + u_{j-1}}{2}\right)\left(\frac{v_j + v_{j-1}}{2}\right)\right)\\ &+ \frac{\phi_4}{\phi_2}M\left(\frac{u_j + u_{j-1}}{2}\right) + \frac{1}{\phi_1\phi_2}K\left(\frac{u_j + u_{j-1}}{2}\right) = 0\end{aligned} \tag{4.10}$$

$$\begin{aligned}&\left(\frac{t_j - t_{j-1}}{h}\right)\left(1 + \epsilon\left(\frac{\theta_j + \theta_{j-1}}{2}\right) + \frac{1}{\phi_5}PrNr\right) + \epsilon\left(\frac{t_j + t_{j-1}}{2}\right)^2\\ &+ Pr\frac{\phi_3}{\phi_5}\left[\left(\frac{f_j + f_{j-1}}{2}\right)\left(\frac{t_j + t_{j-1}}{2}\right)\right]\\ &+ Pr\frac{\phi_3}{\phi_5}\left[-\left(\frac{u_j + u_{j-1}}{2}\right)\left(\frac{\theta_j + \theta_{j-1}}{2}\right)\right.\\ &\left.-A\left\{\left(\frac{\theta_j + \theta_{j-1}}{2}\right) + \frac{\eta}{2}\left(\frac{t_j + t_{j-1}}{2}\right)\right\}\right] = 0\end{aligned} \tag{4.11}$$

In the above discussion, for the $(i+1)-th$ iterate, we write

$$()_j^{(i+1)} = ()_j^{(i)} + \delta()_j^{(i)}, \tag{4.12}$$

by this substitution in Eqs(4.7)-(4.11) and dropping the quadratic and higher terms of δ_j^i, a linear tri-diagonal system will be obtained as follows,

$$\delta f_j - \delta f_{j-1} - \frac{1}{2}h(\delta u_j + \delta u_{j-1}) = (r_1)_{j-\frac{1}{2}}, \tag{4.13}$$

$$\delta u_j - \delta u_{j-1} - \frac{1}{2}h(\delta v_j + \delta v_{j-1}) = (r_2)_{j-\frac{1}{2}}, \tag{4.14}$$

$$\delta\theta_j - \delta\theta_{j-1} - \frac{1}{2}h(\delta t_j + \delta t_{j-1}) = (r_3)_{j-\frac{1}{2}}, \tag{4.15}$$

$$\begin{aligned}&(a_1)_j\delta f_j + (a_2)_j\delta f_{j-1} + (a_3)_j\delta u_j + (a_4)_j\delta u_{j-1} + (a_4)_j\delta u_{j-1}\\ &+ (a_5)_j\delta v_j + (a_6)_j\delta v_{j-1} + (a_7)_j\delta\theta_j + (a_8)_j\delta\theta_{j-1} + (a_9)_j\delta t_j\\ &+ (a_{10})_j\delta t_{j-1} = (r_4)_{j-\frac{1}{2}},\end{aligned} \tag{4.16}$$

$$\begin{aligned}&(b_1)_j\delta f_j + (b_2)_j\delta f_{j-1} + (b_3)_j\delta u_j + (b_4)_j\delta u_{j-1} + (b_4)_j\delta u_{j-1}\\ &+ (b_5)_j\delta v_j + (b_6)_j\delta v_{j-1} + (b_7)_j\delta\theta_j + (b_8)_j\delta\theta_{j-1} + (b_9)_j\delta t_j\\ &+ (b_{10})_j\delta t_{j-1} = (r_5)_{j-\frac{1}{2}},\end{aligned} \tag{4.17}$$

where

$$(r_1)_{j-\frac{1}{2}} = -f_j + f_{j-1} + \frac{h}{2}(u_j + u_{j-1}), \quad (4.18)$$

$$(r_2)_{j-\frac{1}{2}} = -u_j + u_{j-1} + \frac{h}{2}(v_j + v_{j-1}), \quad (4.19)$$

$$(r_3)_{j-\frac{1}{2}} = -\theta_j + \theta_{j-1} + \frac{h}{2}(t_j + t_{j-1}), \quad (4.20)$$

$$\begin{aligned}(r_4)_{j-\frac{1}{2}} = &-h\left[-A\left(\frac{u_j+u_{j-1}}{2}+\eta\frac{v_j-v_{j-1}}{4}\right)+\left(\frac{u_j+u_{j-1}}{2}\right)^2\right.\\ &\left.-\left(\frac{f_j+f_{j-1}}{2}\right)\left(\frac{v_j+v_{j-1}}{2}\right)\right]-h\left[-\frac{1}{\phi_1\phi_2}\left(\frac{v_j-v_{j-1}}{h}\right)\right.\\ &+\beta\left(\left(\frac{f_j+f_{j-1}}{2}\right)^2\left(\frac{v_j-v_{j-1}}{h}\right)\right.\\ &\left.\left.-2\left(\frac{f_j+f_{j-1}}{2}\right)\left(\frac{u_j+u_{j-1}}{2}\right)\left(\frac{v_j+v_{j-1}}{2}\right)\right)\right]\\ &-h\left[\frac{\phi_4}{\phi_2}M\left(\frac{u_j+u_{j-1}}{2}\right)+\frac{1}{\phi_1\phi_2}K\left(\frac{u_j+u_{j-1}}{2}\right)\right], \quad (4.21)\end{aligned}$$

$$\begin{aligned}(r_5)_{j-\frac{1}{2}} = &-h\left[\frac{(t_j-t_{j-1})\left(1+\epsilon\left(\frac{\theta_j+\theta_{j-1}}{2}\right)+\frac{1}{\phi_5}PrNr\right)}{h}\right.\\ &\left.+\epsilon\left(\frac{t_j+t_{j-1}}{2}\right)^2-\frac{\phi_3}{\phi_5}PrA\left(\frac{\theta_j+\theta_{j-1}}{2}+\eta\frac{t_j+t_{j-1}}{2}\right)\right]\\ &-h\frac{\phi_3}{\phi_5}Pr\left[\left(\frac{(f_j+f_{j-1})(t_j+t_{j-1})}{4}\right)\right.\\ &\left.-\left(\frac{(\theta_j+\theta_{j-1})(u_j+u_{j-1})}{4}\right)\right], \quad (4.22)\end{aligned}$$

subject to the boundary conditions

$$\delta f_0 = 0, \delta u_0 = 0, \delta t_0 = 0, \delta u_J = 0, \delta\theta_J = 0, \quad (4.23)$$

the system of linear Eqs(4.12)-(4.17) can be written in matrix form

$$A\delta = b, \quad (4.24)$$

$$A = \begin{bmatrix} A_1 & C_1 & & & & \\ B_2 & A_2 & C_2 & & & \\ & \ddots & \ddots & \ddots & & \\ & & \ddots & \ddots & \ddots & \\ & & & B_{J-1} & A_{J-1} & C_{J-1} \\ & & & & B_J & A_J \end{bmatrix},$$

$$\delta = \begin{bmatrix} \delta_1 \\ \delta_2 \\ \vdots \\ \delta_{j-1} \\ \delta_j \end{bmatrix}, b = \begin{bmatrix} (r_1)_{j-\frac{1}{2}} \\ (r_2)_{j-\frac{1}{2}} \\ \vdots \\ (r_{J-1})_{j-\frac{1}{2}} \\ (r_J)_{j-\frac{1}{2}} \end{bmatrix}. \quad (4.25)$$

Where A is $J \times J$ block tridiagonal matrix with each block size of 5×5. Whereas δ and b are column matrices with J rows. We, then apply the LU factorization to find the solution of δ.

The physical quantities of interest governed the flow are the Skin frication (C_f) and the local Nusselt number (Nu_x), and are defined as: (See for example Abel *et al.*[48])

$$C_f = \frac{\tau_w}{\rho_f U_w^2}, \qquad Nu_x = \frac{xq_w}{k_f(T_w - T_\infty)} \quad (4.26)$$

where τ_w and q_w are the heat flux which is given by

$$\tau_w = -\mu_{nf}\left(\frac{\partial u}{\partial y}\right)_{y=0}, \; q_w = -k_{nf}\left(1+\frac{16\sigma^\star T_{\infty^3}}{3k^\star k_f}\right)\left(\frac{\partial T}{\partial y}\right)_{y=0} \quad (4.27)$$

Applying the non-dimensional transformations (3.2), one obtains

$$C_f Re_x^{\frac{1}{2}} = -\frac{f''(0)}{(1-\phi)^{2.5}}, \quad Nu_x Re_x^{-\frac{1}{2}} = -\frac{k_{nf}}{k_f}(1+Nr)\,\theta'(0) \quad (4.28)$$

where C_f and Nu_r are the reduced Skin frication and Nusselt number respectively. $Re_x = \frac{U_w x}{\nu_f}$ is the local Reynolds number based on the stretching velocity U_w.

To check the validity of our numerical scheme we compare our results to those already available in the literature [49–52] as the especial case for our study. The test case is the natural convection boundary layer flow of fluid over a flat plate with Newtonian slip. Results have been obtained for $\beta = 0$, $A = 0$, $M = 0$, $K = 0$ $\phi = 0$, $\Lambda = 0$, $\epsilon = 0$, $S = 0$, $Nr = 0$ and $B_i \to \infty$. The comparison is shown in Table (1) and are found to be in an excellent agreement. Thus, we are very much confident that the present results are accurate.

5 Entropy generation analysis

Wastage of useful energy ia a part of concern for scientists and engineers. It becomes important to analyze the entropy generation in the system that involves to the irreversibility of useful energy, magnetohydrodynamics is one of the non-ideal effects which is responsible for increasing the entropy of the system. In our case, the actual entropy generation in the nanofluids is given by (See for example Das *et al.*[53])

$$\begin{aligned}E_G = &\frac{k_{nf}}{T_\infty^2}\left\{\left(\frac{\partial T}{\partial y}\right)^2+\frac{16\sigma^\star T_\infty^3}{3k^\star}\left(\frac{\partial T}{\partial y}\right)^2\right\}\\ &+\frac{\mu_{nf}}{T_\infty}\left(\frac{\partial u}{\partial y}\right)^2+\frac{\sigma_{nf}B_0^2(t)u^2}{T_\infty}+\frac{\mu_{nf}u^2}{T_\infty}. \quad (5.1)\end{aligned}$$

In the entropy equation the first term represents the heat transfer irreversibility and the second term is due to the

Table 1: Values of Skin friction coefficient and Nusselt number for Newtonian slip flow

Pr	$Grubka$ Results[49]	Ali Results[50]	$Ishak$ Results[51]	$Nazar$ Results[52]	$Present$ Results
0.72	0.8086	0.8058	0.8086	0.8086	0.8086
1.0	1.0000	0.9961	1.0000	1.0000	1.0000
3.0	1.9237	1.9144	1.9236	1.9237	1.9237
7.0	-	-	3.0722	3.0723	3.0723
10	3.7207	3.7006	3.7206	3.7207	3.7207

fluid friction and the third term is because of magnetohydrodynamic effect and porous medium. The dimensionless entropy generation is represented by N_G and is defined as

$$N_G = \frac{{T_\infty}^2 c^2 E_G}{k_f\,(T_w - T_\infty)^2}. \tag{5.2}$$

From Equation (3.4), we can achieve the entropy equation in the dimensionless form as

$$N_G = Re\left[\phi_5(1+Nr)\theta'^2 + \frac{1}{\phi_1}\frac{B_r}{\Omega}\left(f''^2 + \phi_1\phi_4 M f'^2 + K f'^2\right)\right], \tag{5.3}$$

here Re represents the Reynolds number, B_r represents the Brinkmann number and the dimensional less temperature gradient that can represented by Ω, which is defined by

$$R_e = \frac{U_w L^2}{\nu_f x}, \qquad B_r = \frac{\mu_f U_w^2}{k_f\,(T_w - T_\infty)}, \qquad \Omega = \frac{T_w - T_\infty}{T_\infty}. \tag{5.4}$$

6 Numerical results and discussion

Numerical results in the form of graphs and tables for chosen values of some physical parameters are presented in this section. The results are produce for the Cu-water and TiO_2-water non-Newtonian Maxwell nanofluids. The discussion is focused on the thermal enhancement in nanofluids and comparison can be drawn on the behavior of two different type of nanofluids. The numerical results are presented in Figs. (3)-(22) and in Table (3). The material properties of Cu–water and TiO_2-water nanofluids are tabulated in Table 2 (Sharma *et al.* [54]).

The effects of Maxwell parameter β on velocity, temperature and entropy generation profiles of Cu-water and TiO_2-water non-Newtonian Maxwell nanofluids are presented in Figures (3)-(5). Computations are performed for $\beta = 1.0, 5.0, 10.0$ at uniform nanoparticle concentration of 0.2. The velocity profiles in Figure (3) decreases with an increasing values of β and hence decreases the thickness of momentum boundary layer. Moreover, for the

Table 2: Thermophysical properties of Base Fluid and Nanoparticles

Thermophysical properties	ρ (kgm^{-3})	c_p $(JKg^{-1}K^{-1})$	k $(Wm^{-1}K^{-1})$
Pure water (H_2O)	997.1	4179	0.6130
Copper (Cu)	8933	385.0	401.00
Copper oxide (CuO)	6320	531.8	76.500
Alumina (Al_2O_3)	3970	765.0	40.000
Titanium oxide (T_iO_2)	4250	686.2	8.9538

fixed value of $\beta = 0.3$ the boundary layer thickness of TiO_2-water nanofluid is relatively more than the Cu-water nanofluid. The decreasing trend in velocity profiles is due to increase of resistance in fluid and also corresponds to increase in skin friction coefficient (velocity gradient) at the boundary. It can be seen from Figure (4) that the temperature of nanofluids rises with the increasing values of parameter β. This increasing trend indicate the enhancement in the thickness of thermal boundary layer and reduction in the rate of heat transfer. The reason behind this behaviour of temperature profiles is the increase in the elasticity stress parameter. Figure (5) shows the impact of Maxwell parameter β on the entropy of the system. It is noticed that increasing Maxwell parameter increases the entropy of the system. Finally, it is observed from Table (3), the rate of heat transfer at the boundary (Nusselt number) decreases for both Cu and TiO_2 water based nanofluids.

Figures (6)-(8) depicted the influence of unsteady parameter A on velocity, temperature and entropy generation profiles of Maxwell nanofluid. It is found that the fluid flow slowly (Figure (6)) and its temperature decrease within boundary layer with ascending values of parameter A (Figure (7)). The effect of increasing values of parameter A is to decrease the thickness of both momentum and thermal boundary layer thickness. Figure (8) displays the influence of variation of unsteadiness parameter A on the entropy generation. It is observed (at about $\eta = 0.3$) the entropy profiles show the cross-over point. Before this point the entropy is increasing and after this it starts decreasing. From Table (3), the increasing trends are observed for

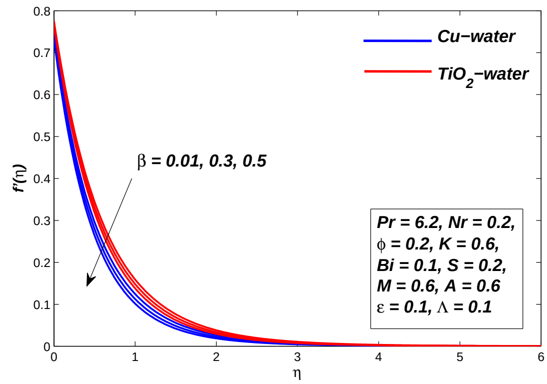

Figure 3: Velocity distribution against the parameter β

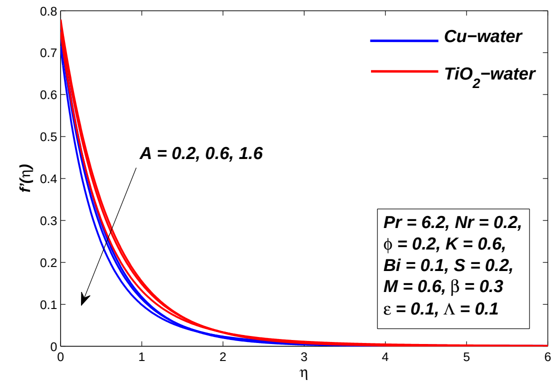

Figure 6: Velocity distribution against the parameter A

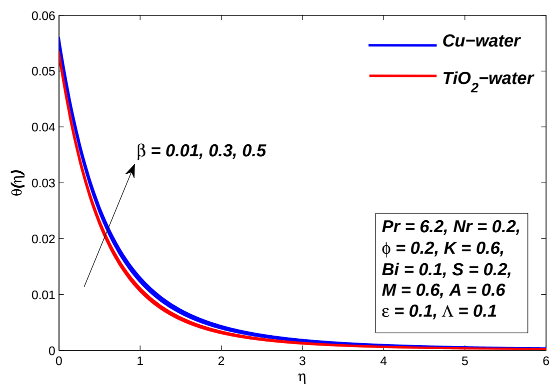

Figure 4: Temperature distribution against the parameter β

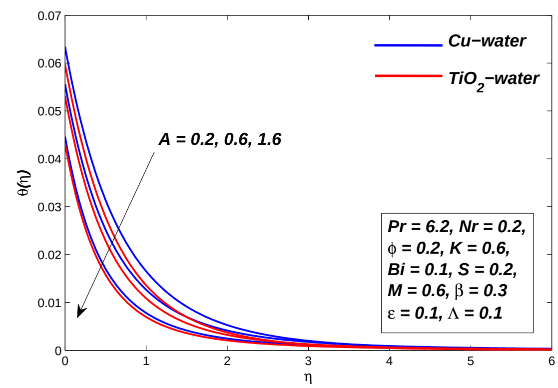

Figure 7: Temperature distribution against the parameter A

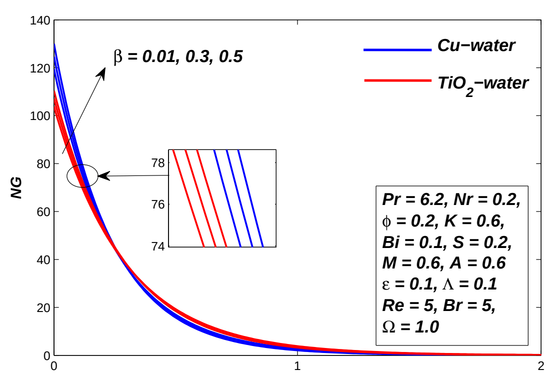

Figure 5: Entropy generation against the parameter β

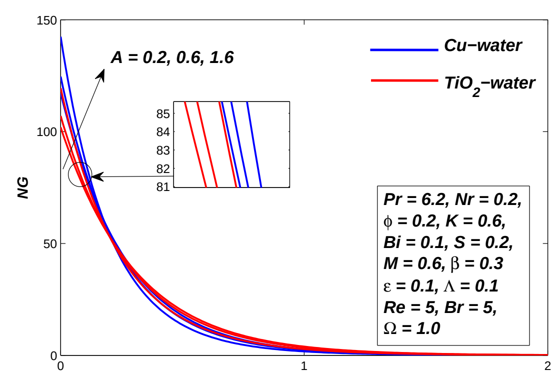

Figure 8: Entropy generation against the parameter A

the velocity and temperature gradients at the boundary. The boundary layer energy is absorbed due to unsteadiness resulting the increase in the rate of heat transfer at the boundary.

Figures (9)-(14) exhibited the behaviours of nanofluids motion, temperature distribution and entropy generation with increasing strength of applied transverse magnetic field and the porosity of the medium respectively. Similar behaviours are observed in profiles of velocity, temperature and entropy with increasing values of parameter M and K. The magnetic field applied normal to the flow direction, produces a resistive force known as Lorentz force which reduces the fluid motion within the boundary layer. The Lorentz force impact in the form of decreasing trend in velocity profiles are clearly visible in Figure (9). Whereas the increase in permeability is to decrease the magnitude of the resistive Darcian body force, therefore a continuous less drag is experienced by the fluid and flow reduces thereby declines the velocity within boundary layer (12). The parameters M and K are inversely proportional to the density of nanofluid hence the increase in the strength of applied magnetic field or the permeability of the medium reduces the density and as a result the temperature of the fluid rises within boundary layer (Figs. (10), (13)). This will increase the thickness of thermal boundary layer and reduces the rate of heat transfer. The influence of Lorentz or the Darcian body force at the boundary is presented in Table (3). The Skin friction coefficient increases but the Nusselt number decreases with increasing strength of parameters M and K. Figure (11), (14) demonstrated that the entropy of the system increases with increase in the strength of applied transverse magnetic field and the permeability of the medium.

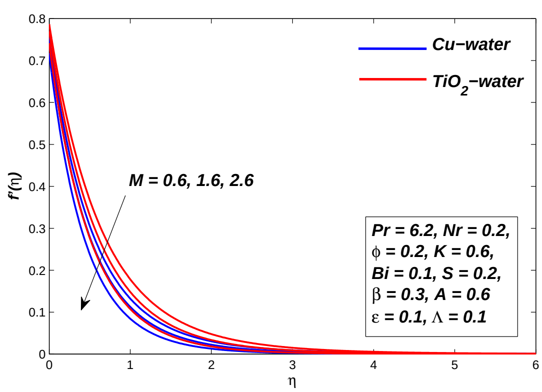

Figure 9: Velocity distribution against the parameter M

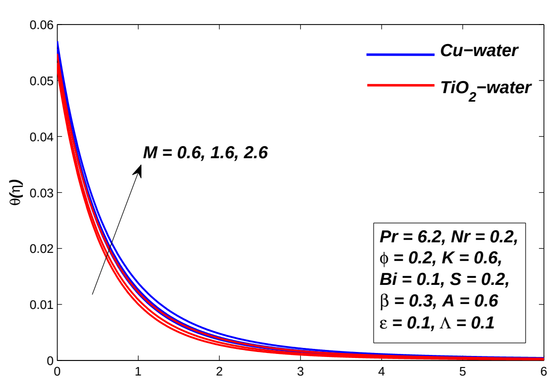

Figure 10: Temperature distribution against the parameter M

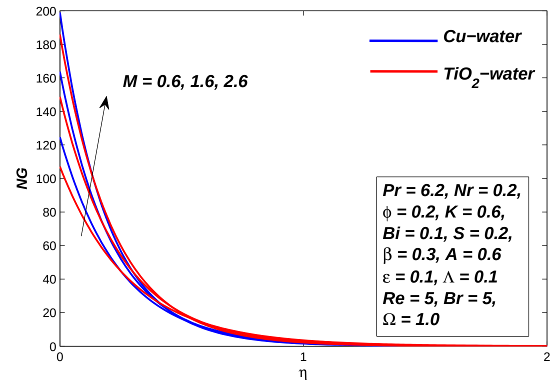

Figure 11: Entropy generation against the parameter M

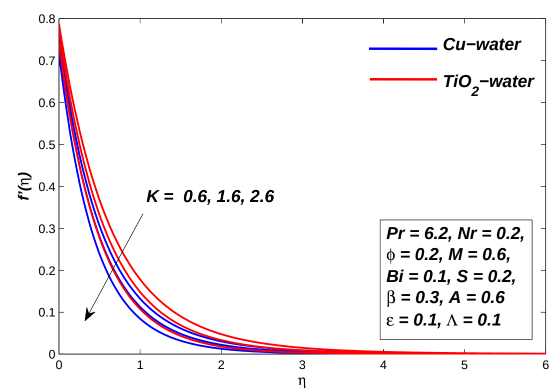

Figure 12: Velocity distribution against the parameter K

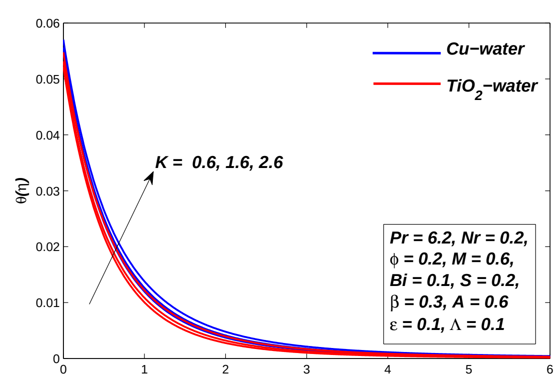

Figure 13: Temperature distribution against the parameter K

Figures (15)-(17) displayed respectively the nature of fluid motion, temperature distribution and entropy gener-

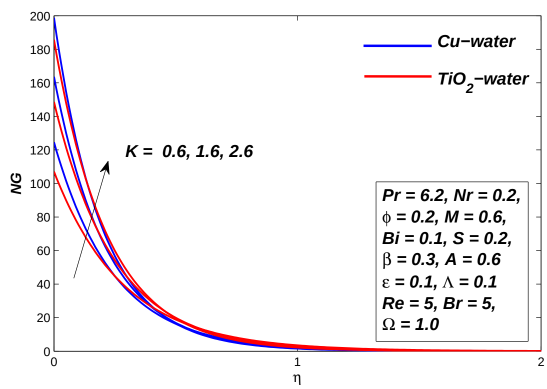

Figure 14: Entropy generation against the parameter K

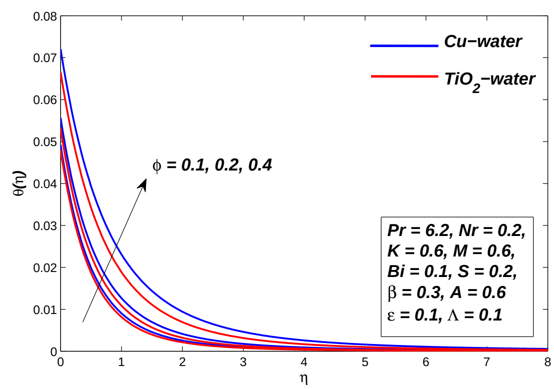

Figure 16: Temperature distribution against the parameter ϕ

ation within boundary layer for Maxwell nanofluids due to variation in nanoparticle volume concentration parameter ϕ. It is found that the nanofluid velocity decreases and the temperature increases with increasing values of parameter ϕ. These figures are in agreement with the physical behavior that the denser nanoparticle volume fraction causes thinning of momentum boundary layer and the rate of heat transfer also reduces within boundary layer. The increase in volume of nanoparticles increases the overall thermal conductivity of nanofluids because the solid particles have higher thermal conductivity as compared to base fluid. The increase in thermal conductivity is responsible for decrease in thickness of momentum boundary layer. Whereas the increase in overall thermal conductivity of nanofluids raises the temperature and boundary layer thickness. The increasing and decreasing trend in velocity and temperature gradient respectively at the boundary are observed with increase in parameter ϕ Table (3). In Figure (17) depicts increasing nanoparticle volume fraction Parameter ϕ the entropy of the system is also increases.

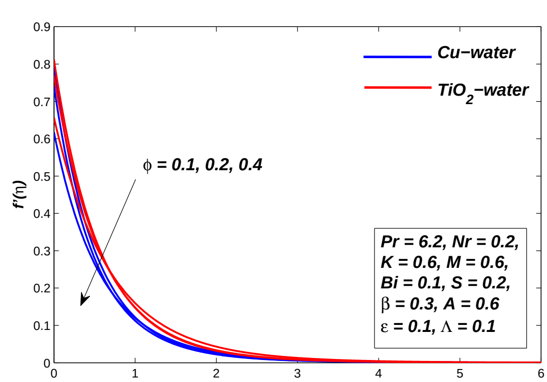

Figure 15: Velocity distribution against the parameter ϕ

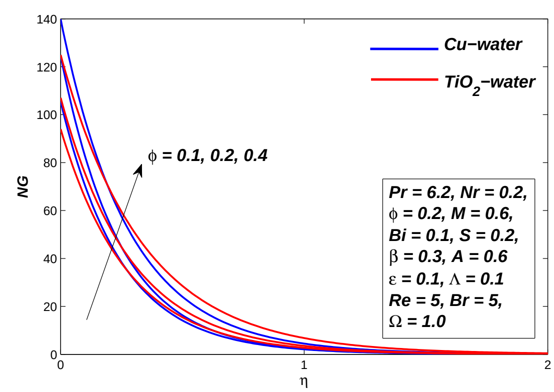

Figure 17: Entropy generation against the parameter ϕ

Figures (18)-(20) showed the positive values of slip parameter Λ, slows down the fluid motion and entropy generation but raise the temperature of Maxwell nanofluids. The decrease in velocity is obvious because the increase in lubrication and slipperiness at the surface retards the flow and the stretching pull can be only partly transmitted to the fluid. As a result the thickness of momentum boundary layer will decreases with increase in parameter Λ. On the other hand, slipperiness affects the temperature of the fluid inversely; that is, the temperature of the nanofluid enhances within the boundary layer. Table (3) shows the increase in Λ, leads to decrease in skin friction coefficient for both Cu and TiO_2 water based nanofluids. This was expected to happen due to the fact that slip effects reduces the friction at the solid-fluid interface and thus reduce skin friction coefficient. The reduction in Nusselt number or the heat transfer rate at the boundary is observed from Table (3) with increase in slip. Increasing velocity slip parameter Λ is analyzed in Figure (20). It is noteworthy that the entropy decreases by increasing the values of Λ.

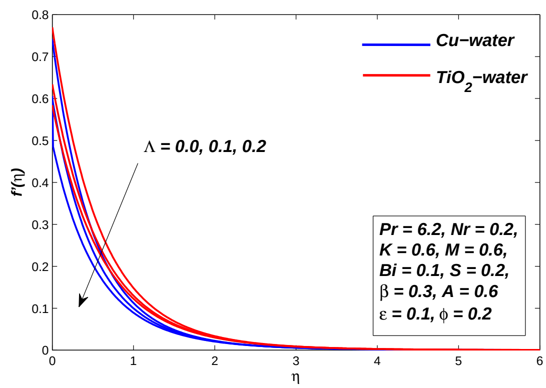

Figure 18: Velocity distribution against the parameter Λ

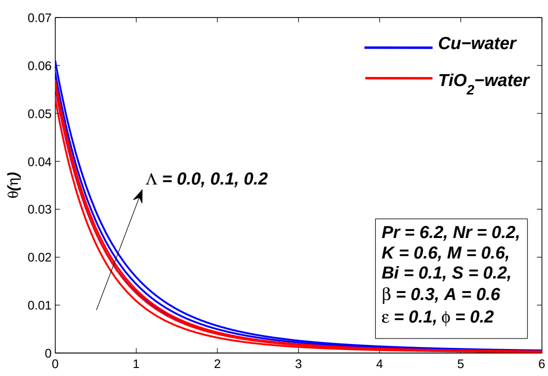

Figure 19: Temperature distribution against the parameter Λ

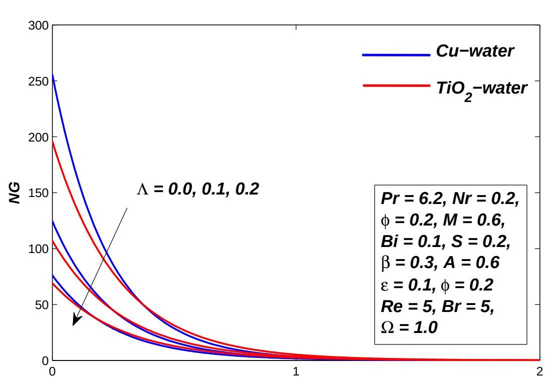

Figure 20: Entropy generation against the parameter Λ

Figure (21) shows the impact of Reynolds number on the entropy of the system. It is noticed that increasing Reynolds number Re increase the entropy of the system. The physical reason for this observation is that for higher Reynolds number the inertial forces dominates the viscous forces thus the entropy of the system rises. Figure (22) discusses the influence of Brinkman number on the entropy of the system. It is observed that increasing the values of Br increases the temperature and hence the entropy of the system.

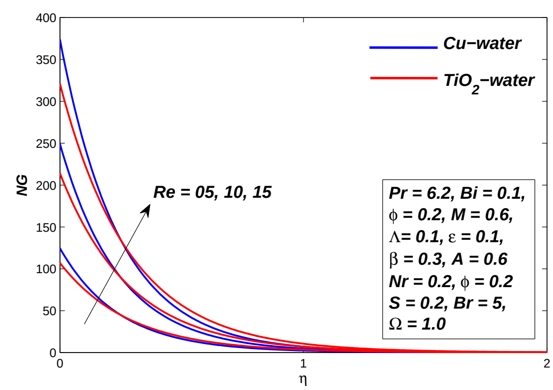

Figure 21: Entropy generation distribution against the parameter Re

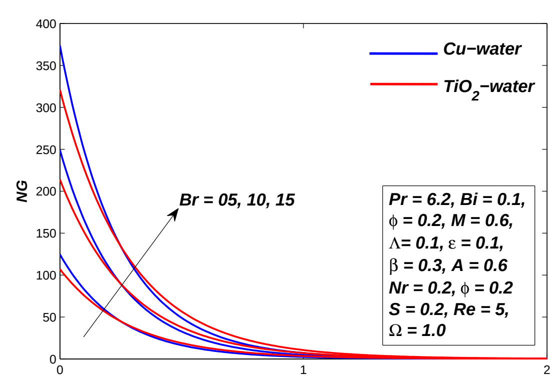

Figure 22: Entropy generation distribution against the parameter Br

7 Conclusions

The present research analyzed the heat transfer capabilities and the entropy generation of non-Newtonian Maxwell nanofluid in the presence of slip and convective

Table 3: Values of Skin Friction = $C_f Re_x^{\frac{1}{2}}$ and Nusselt Number = $N_u Re_x^{\frac{-1}{2}}$ for $Pr = 6.2$

β	A	M	K	ϕ	Λ	ϵ	Nr	Bi	S	$C_f Re_x^{\frac{1}{2}}$ Cu – $water$	$C_f Re_x^{\frac{1}{2}}$ T_iO_2 – $water$	$N_u Re_x^{\frac{-1}{2}}$ Cu – $water$	$N_u Re_x^{\frac{-1}{2}}$ T_iO_2 – $water$
0.01	0.6	0.6	0.6	0.2	0.1	0.1	0.2	0.1	0.2	2.4702	2.2194	0.0650	0.0718
0.3										2.5859	2.3025	0.0649	0.0716
0.5										2.6656	2.3592	0.0648	0.0715
0.3	0.2									2.4713	2.2125	0.0644	0.0711
	0.6									2.5859	2.3025	0.0649	0.0716
	1.6									2.8408	2.5061	0.0657	0.0723
		0.6								2.5859	2.3025	0.0649	0.0716
		1.6								2.8225	2.5862	0.0648	0.0714
		2.6								3.0215	2.8159	0.0647	0.0713
			0.6							2.5859	2.3025	0.0649	0.0716
			1.6							2.8221	2.5858	0.0648	0.0714
			2.6							3.0290	2.8152	0.0647	0.0713
				0.1						2.0461	1.8795	0.0857	0.0901
				0.2						2.5859	2.3025	0.0649	0.0716
				0.4						2.8253	3.4338	0.0373	0.0455
					0.0					3.7682	3.1669	0.0652	0.0718
					0.1					2.5859	2.3025	0.0649	0.0716
					0.2					1.9998	1.8309	0.0647	0.0713
						0.1				2.5859	2.3025	0.0649	0.0716
						1.0				2.5859	2.3025	0.0648	0.0715
						2.0				2.5859	2.3025	0.0647	0.0714
							0.2			2.5859	2.3025	0.0649	0.0716
							0.5			2.5859	2.3025	0.0796	0.0877
							0.8			2.5859	2.3025	0.0939	0.1035
								0.1		2.5859	2.3025	0.0649	0.0716
								0.2		2.5859	2.3025	0.1230	0.1359
								0.6		2.5859	2.3025	0.3041	0.3385
									0.2	2.5859	2.3025	0.0649	0.0716
									0.5	3.0447	2.5977	0.0655	0.0722
									0.6	3.2456	2.7177	0.0656	0.0724

boundary conditions. Thermal radiation and the temperature dependent thermal conductivity are also considered in the present model and the uniform magnetic field is applied in the transverse direction to the flow. The mathematical formulation is carried out through a boundary layer approach and the numerical computations are carried out for Cu-water and TiO_2-water nanofluids. The results are summarized on the basis of variation in nanofluid's motion, temperature distribution and entropy generation within boundary layer.

The key parameters such as, non-Newtonian Maxwell fluid parameter, strength of the applied magnetic field, permeability, nanoparticle volumetric concentration, variable thermal conductivity, velocity slip and thermal radiation increases the temperature distribution within the boundary layer. This will increase the thickness of thermal boundary layer and reduce the rate of heat transfer at the surface. This will increase the overall entropy of the system and decreases the fluid motion within boundary layer. The unsteadiness parameter and the suction parameter at the boundary reduces the thickness of the thermal boundary layer and increases the rate of heat transfer at the surface.

The highlight of the study, entropy of the system is observed to enhance with the increase in the values of Reynolds number Re, Brinkmann number Br, unsteadiness parameter A, magnetic parameter M, permeability parameter K, nanoparticle volume fraction Parameter ϕ and suction parameter $S > 0$ but reduce with increase in the values of injection parameter $S < 0$ and velocity slip Parameter Λ. Finally, the Cu-water based nanofluid is observed as better thermal conductor than TiO_2-water based nanofluid.

In future the present qualitative analysis can be quantified to calculate the thermal efficiency of solar collectors and can be generalized to include the effects of variable viscosity, variable porosity, multidimensional MHD slip flow and heat transfer of non-Newtonian and regular nanofluids.

References

[1] Nagarajan P.K., Subramani J., Suyambazhahan S., Sathyamurthy R., Nanofluids for solar collector applications: A Review, 6th Int. Conf. Appl. Energ.-ICAE, Energ. Proced., 2004, 61, 2416-2434.

[2] Kalogirou S., The potential of solar industrial process heat applications, Appl. Energ., 2003, 76, 337-361.

[3] Aste N., Beccali M., Tagliabue L.C., Nomograph for rapid technical and economic assessment of solar thermal systems for DHW production, Sol. Energy., 2012, 86, 2475-2485.

[4] Pei G., Li J., Ji J., Analysis of low temperature solar thermal electric generation using regenerative Organic Rankine Cycle, Appl. Ther. Eng., 2010, 30, 998-1004.

[5] Wang M., Wang J., Zhao Y., Zhao P., Dai Y., Thermodynamic analysis and optimization of a solar-driven regenerative organic Rankine cycle (ORC) based on flatplate solar collectors, Appl. Ther. Eng., 2013, 50, 816-825.

[6] Kalogirou S.A., Solar thermal collectors and applications, Prog. Energy. Comb. Sci., 2004, 30, 231-295.

[7] Nagarajan P.K., Subramani J., Suyambazhahan S., Sathyamurthy R., Nanofluids for solar collector applications: A review, Enrgy. Proced., 2004, 61, 2416

[8] Chaji H., Ajabshirchi Y., Esmaeilzadeh E., Heris S.Z., Hedayati zadeh M., Kahani M., Experimental study on thermal eflciency of flat plate solar collector using TiO_2 water nanofluid, Mod. Appl. Sci., 2013, 7, 1852-1913.

[9] Ghasemi S.E., Ahangar G.H.R.M., Numerical analysis of performance of solar parabolic trough collector with Cu-Water nanofluid, Int. J. NanoDime., 2014, 5, 233-240.

[10] Sharma K., Kundan L., Nanofluid Based Concentrating Parabolic Solar Collector (NBCPSC): A New Alternative, Int. J. Res. Mech. Eng. Tech., 2014, 4, 2249-5762.

[11] Bellos E., Tzivanidis C., Antonopoulos K.A., Gkinis G., Thermal enhancement of solar parabolic trough collectors by using nanofluids and converging-diverging absorber tube, Renew. Energ., 2016, 94, 213-222.

[12] Tong Y., Kim J., Cho H., Effects of thermal performance of enclosed-type evacuated U-tube solar collector with multi-walled carbon nanotube/water nanofluid, Renew. Energ., 2015, 83, 463-473.

[13] Kim H., Ham J., Park C., Cho H., Theoretical investigation of the efficiency of a U-tube solar collector using various nanofluids, Energy., 2016, 94, 497-507.

[14] Muhammad M.J., Muhammad I.A., Sidik N.A., Yazid A.W.M., Thermal performance enhancement of flat-plate and evacuated tube solar collectors using nanofluid: A review, Int. Commun. Heat. Mass., 2016, 76, 6-15.

[15] Ellahi R., Hassan M., Zeeshan A. A study of heat transfer in power law nanpfluid, Therm. Sci., 2016, 20, 2015-2026.

[16] Ellahi R., Hassan M., Zeeshan A., Khan A.A, The shape effects of nanoparticles suspended in HFE-7100 over wedge with entropy generation and mixed convection, Appl. Nano. Sci., 2016, 6, 641-651.

[17] Sheikholeslami M., Zia Q.M.Z., Ellahi R., Influence of In- duced Magnetic Field on Free Convection of Nanofluid Considering Koo-Kleinstreuer-Li (KKL) Correlation, Appl. Sci., 2016, 6(11), 324

[18] Esfahani J.A., Akbarzadeh M., Rashidi S., Rosen M.A., Ellahi R., Influences of wavywall and nanoparticles on entropy generation over heat exchanger plat, Int. J. Heat. Trans., 2017, 109, 1162-1171.

[19] Rahman S.U., Ellahi R., Nadeem S., Zia Q.M.Z., Simultaneous effects of nanoparticles and slip on Jeffrey fluid through tapered artery with mild stenosis, J. Mol. Liq., 2016, 218, 484-493.

[20] Bhatti M.M., Zeeshan A., Ellahi R., Endoscope analysis on peristaltic blood flow of sisko fluid with titanium magnetonanoparticles, Comp. Biol. Med., 2016, 78, 29-41.

[21] Bhatti M.M., Zeeshan A., Ellahi R., Simultaneous effects of coagulation and variable magnetic field on peristaltically induced motion of Jeffrey nanofluid containing gyrotactic microorganism, Microvasc Res., 2017, 110, 32-42.

[22] Tyagi S.K., Wang S.W., Singhal M.K., Kaushik S.C., Park S.R., Exergy analysis and parametric study of concentrating type solar collectors, Int. J. Ther. Sci., 2007, 46, 1304-1310.

[23] Liu G., Cengel Y.A., Turner R.H., Exergy analysis of a solar heating system, J. Sol. Energ., 1995, 117, 249-251.

[24] Reyes E.T., Cervantes de Gortari J.G., Ibarra-Salazar B.A., Picon-Nunez M.A., design method of flat-plate solar collectors based on minimum entropy generation, Exergy., 2001, 1, 46-52.

[25] Bejan A., Keary D.W., Kreith F., Second law analysis and synthesis of solar collector systems, J. Sol. Energ., 1981, 103, 23-28.

[26] Suzuki A., A fundamental equation for exergy balance on solar collectors, J. Sol. Energ., 1988, 110, 102-106.

[27] Farzad J., Emad A., Energetic and exergetic evaluation of flat plate solar collectors, Renew. energ., 2013, 56, 65-63.

[28] Luminosua I., Fara L., Determination of the optimal operation mode of a flat solar collector by exergetic analysis and numerical simulation, Energy., 2005, 30, 731-747.

[29] Farahat S., Sarhaddi F., Ajam H., Exergetic optimization of flat plate solar collectors, Renew. Energ., 2009, 34, 1169-1174.

[30] Nasrin R., Parvin S., Alim M.A., Heat Transfer and Collector Efficiency through a Direct Absorption Solar Collector with Radiative Heat Flux Effect, Numer. Heat. Transfer., 2015, 68, 887-907.

[31] Said Z., Alim M. A., Janajreh I., Exergy eflciency analysis of a flat plate solar collector using graphene based nanofluid, Mater. Sci. Eng., 2015, 92

[32] Yejjer O. ,Kolsi L., Aich W., Rashed A.A., Borjini M.N., Aissia H. B., Study of three-dimensional natural convection and entropy generation in an inclined solar collector equipped with partitions, Wiley, 2017

[33] Moghadam M.C., Edalatpour M., Solano J.P., Numerical study on conjugated laminar mixed convection of alumina/water nanofluid flow, heat transfer, and entropy generation within a tube-on-sheet flat plate solar collector, J. Sol. Energ., 2017

[34] Gupta M.K., Kaushik S.C., Exergetic performance evaluation and parametric studies of solar air heater, Energy., 2017

[35] Santra A.K., Sen S., Chakraborty N., The forced convection of Cu-water nanfluid in a channel with both Newtonian and Non-Newtonian models. Int. J. Ther. Sci., 2009, 48, 391-400.

[36] Hussain S.T., Nadeem S., Haq R.Ul., Model-based analysis of micropolar nanofluid flow over a stretching surface, Euro. Phys. J. Plus., 2014, 45, 161

[37] Aziz T., Aziz A., Khalique C.M., Exact solutions for stokes flow of a non-newtonian nanofluid model: a lie similarity approach, Z. Naturforsch., 2016

[38] Shehzad S.A., Abdullah Z., Alsaedi A., Abbaasi F.M., Hayat T., Boundary thermally radiative three-dimensional flow of Jeffrey nanofluid with internal heat generation and magnetic field, J. Magn. Magn. Mater., 2016, 397, 108-114.

[39] Ramzan M., Bilal M., Chung J.D., Farooq U., Mixed convective flow of Maxwell nanofluid past a porous vertical stretched surface - An optimal solution, Results. Phys., 2015, 6, 1072-1079.

[40] Hayat T., Hussain T., Shezad S.A., Alsaedi A., Flow of Oldroyd-B fluid with nanoparticles and thermal radiation, Appl. Math. Mech., 2015, 36, 69-80.

[41] Farooq U., Hayat T., Alsaedi A., Liao S., Heat and mass transfer of two-layer flows of third-grade nano-fluids in a vertical channel, Appl. Math. Comp., 2016, 242, 528-540.

[42] Mukhopadhyay S., Heat Transfer Analysis of the unsteady flow of a Maxwell fluid over a stretching surface in the presence of a heat source/sink, Chinese. Phys. Soci., 2012, 29

[43] Bhaskar N., Reddy P.S., Poornima T., Sreenivasulu P., Influence of variable thermal conductivity onMHDboundary layar slip flow of ethylene-glycol based Cu nanofluids over a stretching sheet with convective boundary condition, Int. J. Eng. Math., 2014, 1-10.

[44] Arunachalam, Rajappa N.R., Forced convection in liquid metals with variable thermal conductivityand capacity, Acta. Mechl., 1978, 31

[45] Maxwell J., A Treatise on electricity and magneism (second edition), Clar. Press. Oxford. UK., 1881

[46] Brewster M.Q., Thermal radiative transfer and properties, Jo. Wiley. Sons., 1992

[47] Keller H.B., A New Difference Scheme for Parabolic Problems. In: Hubbard, B., Ed., Numerical Solutions of Partial Differential Equations, Acad. Press, New York., 1971, 2, 327-350.

[48] Abel M.S., Tawade J.V., Nandeppanavar M.M., MHD flow and heat transfer for the upper-convected Maxwell fluid over a stretching sheet, Meccanica., 2012, 47, 385-393.

[49] Grubka L.J., Bobba K.M., Heat transfer characteristics of a continuous, stretching surface with variable temperature, ASME, J. Heat. Trans., 1985, 107, 248-250.

[50] Me A., Heat transfer characteristics of a continuous stretching surface. ASME, J. Heat. Trans., 1994, 29, 227-234.

[51] Ishak A., Nazar R., Pop I., Mixed convection on the stagnation point flow towards a vertical, continuously stretching sheet. J. Heat. Trans., 2007, 129, 1087-1090.

[52] Ishak A., Nazar R., Pop I., Boundary layer flow and heat transfer over an unsteady stretching vertical surface. Meccanica., 2009, 44, 369-375.

[53] Das S., Chakraborty S., Jana R.N., Makinde O.D., Entropy analysis of unsteady magneto-nanofluid flow past accelerating stretching sheetwith convective boundary condition, Adv. Appl. Math. Mech., 2015, 36, 1593-1610.

[54] Sharma R., Ishak A., Pop I., Partial slip flow and heat transfer over a stretching sheet in a nanofluid, Math. Probl. Eng., 2013, 2013, 724547.